

## Effective Control of the Charge and Magnetic States of Transition-Metal Atoms on Single-Layer Boron Nitride

Bing Huang,<sup>1</sup> Hongjun Xiang,<sup>2</sup> Jaejun Yu,<sup>3</sup> and Su-Huai Wei<sup>1</sup>

<sup>1</sup>National Renewable Energy Laboratory, 1617 Cole Boulevard, Golden, Colorado 80401, USA

<sup>2</sup>Key Laboratory of Computational Physical Sciences and Department of Physics, Fudan University, Shanghai 200433, People's Republic of China

<sup>3</sup>Center for Strongly Correlated Materials Research, Department of Physics and Astronomy, Seoul National University, Seoul 151-747, Korea

(Received 3 December 2011; published 14 May 2012)

Developing approaches to effectively control the charge and magnetic states is critical to the use of magnetic nanostructures in quantum information devices but is still challenging. Here we suggest that the magnetic and charge states of transition-metal (TM) doped single-layer boron-nitride (SLBN) systems can be easily controlled by the (internal) defect engineering and (external) electric fields ( $E_{\text{ext}}$ ). The relative positions and symmetries of the in-gap levels induced by defect engineering and the TM  $d$ -orbital energy levels effectively determine the charge states and magnetic properties of the TM/SLBN system. Remarkably, the application of an  $E_{\text{ext}}$  can easily control the size of the crystal field splitting of the TM  $d$  orbitals and thus, leading to the spin crossover in TM/SLBN, which could be used as  $E_{\text{ext}}$ -driven nonvolatile memory devices. Our conclusion obtained from TM/SLBN is valid generally in other TM adsorbed layered semiconductors.

DOI: 10.1103/PhysRevLett.108.206802

PACS numbers: 73.61.Ey, 73.22.-f, 75.30.Wx, 75.75.-c

Graphene has many interesting electronic and magnetic properties. Its low-dimensional nature makes it ideally suitable for nanoscale device applications[1]. In particular, graphene has been considered as a promising host material for spintronic related applications because it can possess magnetic moments through defect control such as forming nano ribbons[2,3] or forming vacancies[4], and more importantly, it has low intrinsic spin-orbit interaction and low hyperfine interaction between the electron spins and the carbon nuclei. However, the coupling between the  $2p$ -like magnetic moments through electron or hole carriers, a central requirement of spintronics, is relatively weak. As a result, introducing transition metals (TM) in graphene system has become a popular choice to enhance the magnetic interactions.

Extensive experimental[5–7] and theoretical studies [8–11] have been carried out to test this idea. Indeed, magnetic properties of TM doped graphene can be significantly modified. However, because of the lack of band gap in graphene, the TM  $d$  orbitals strongly couples with the conduction or valence bands of graphene [10,11] and further control of the charge and magnetic states of TM/graphene system is quite difficult [7], but the reliable control of the charge and magnetic states of a magnetic material is a key step for spintronics and quantum information devices [12,13]. Naturally, one may expect to solve this difficulty by replacing metallic graphene layer with some semiconducting layers. Single-layer boron-nitride (SLBN) or other III–V (e.g., AlN and GaN) and II–VI (e.g., ZnO and ZnS) graphiticlike structures have been synthesized in experiments[14,15] or predicted in theories

[16,17]. Owing to the large chemical difference between cation and anion atoms, these ionic-layer structures display large heteropolar band gaps [14,17]. Because the energies of TM  $3d$  orbitals can exist inside the band gap [18], i.e., not in the conduction or valence band as in the case of TM/graphene, we expect that these in-gap TM  $3d$  orbitals may be easier to be controlled by various approaches and the TM/III–V or TM/II–VI layer systems might be considered as preferential magnetic materials for low-dimensional spintronics.

In order to examine the controllability of the magnetic and charge states in these TM/III–V or TM/II–VI layer structures, taking TM/SLBN as a typical example, we have systematically studied  $3d$  TM atoms (from Sc to Zn) doped SLBN based on density-functional theory (DFT) calculations [19]. In general, we find that the magnetic and charge states of TM/SLBN systems can be effectively controlled by the (internal) defect engineering and/or (external) electric fields ( $E_{\text{ext}}$ ). The relative position and symmetry of the in-gap levels induced by structural defects or impurities play a crucial role in determining the charge states and magnetic properties of adsorbed TM atoms. Interestingly, we show that an  $E_{\text{ext}}$  can effectively control the size of the crystal field splitting of the TM  $3d$  orbitals, thus leading to a spin-crossover effect in TM/SLBN systems, which could be used for applications such as nonvolatile memory. Our further calculations show that the conclusions obtained from TM/SLBN systems are valid in other TM/III–V or TM/II–VI layer systems.

An isolated TM atom usually has a  $s^{\uparrow\downarrow} s^{\uparrow\downarrow} d^{m\uparrow} d^{n\downarrow}$  configuration, except for Cr and Cu atoms, where only

one electron occupies the  $4s$  orbital. After adsorption on pristine SLBN, the large Coulomb repulsion between the TM  $4s$  orbital and the SLBN layer pushes up the  $4s$  orbital energy, therefore causing a charge transfer from the TM  $4s$  orbital to the  $3d$  orbital, resulting usually either in  $d^{m+1\uparrow} s^{1\downarrow} d^{m\downarrow} s^{0\downarrow}$  ( $m < 5$ ) or  $d^{m\uparrow} s^{1\uparrow} d^{m+1\downarrow} s^{0\downarrow}$  ( $m \geq 5$ ) spin configurations. Because of the large band gap of BN, there is no charge transfer between TM and pristine SLBN, so all the TM atoms exhibit neutral charge states  $\text{TM}^0$ . This indicates that the magnetic properties of SLBN can be modified by adsorption of TM on its surface, as one would expect. Unfortunately, the calculations show that all TM atoms on SLBN have binding energies less than 1 eV, agreeing with previous calculations [20], which indicates that the TM atoms on the BN surface are quite mobile at room-temperature, like the diffusion of TM atoms on pristine graphene surfaces [21,22].

As learned from the TM/graphene system [10,11,21,23], an effective way to enhance the stability of TM/SLBN systems is to introduce defects in SLBN. These defects lead to a locally increased reactivity and thus enable the formation of stable chemical bonds with adsorbed atoms [21,23,24]. In experiments, vacancies and impurities (e.g., carbon and oxygen) are typically created during the synthesis of SLBN [14,25,26]. Taking boron-vacancy ( $V_B$ ), nitrogen-vacancy ( $V_N$ ), boron-nitrogen-vacancy ( $V_{BN}$ ), and C impurity as examples, we demonstrate here that charge and magnetic states of TM/SLBN can be more easily controlled by defect engineering.

The (local) optimized structures of  $V_B$ ,  $V_N$ , and  $V_{BN}$  are shown in Fig. 1(a). In the case of  $V_B$ , the Jahn-Teller distortion lowers its symmetry from  $D_{3h}$  to  $C_{2v}$  after relaxation [27,28]. The magnetic moments of N atoms at  $V_B$  are 1, 1, and  $-1 \mu_B$ , respectively. The N-N distance between the two N atoms at  $V_B$  with opposite spin direction is 2.70 Å while the distance between the two N atoms with same spin direction is increased to 2.79 Å due to Coulomb repulsion.  $V_N$  has a symmetry of  $D_{3h}$  and the three first-neighbor B-B distances at  $V_N$  are 2.29 Å. The three B atoms at  $V_N$  have same spin directions and they contribute to a total magnetic moment of  $1 \mu_B$ .  $V_{BN}$  ( $C_{2v}$  symmetry) is spin-unpolarized. The first-neighbor B-B and N-N distances at  $V_{BN}$  are 1.93 and 1.81 Å, respectively.

The defect levels of  $V_B$  ( $V_N$ ) at the vacancy site can be classified to have  $a^\pi$ ,  $a^\sigma$ ,  $e^\pi$ , and  $e^\sigma$  representations. In  $V_B$ , the  $a^\pi$ ,  $a^\sigma$ , and  $e^\pi$  states are resonant inside the valence band while  $e^\sigma$  states are above the valence band maximum (VBM) in the gap. Because of the crystal field splitting caused by the Jahn-Teller distortion, the twofold degenerate  $e^\sigma$  states further split into  $b_1^\sigma$  and  $b_2^\sigma$ , as shown in Fig. 1(b). Finally, due to the spin exchange splitting, the occupied  $b_2^\sigma$  state in spin-up channel moves down into the valence band. The three hole levels above valence band make  $V_B$  acting as a triple acceptor. Different from  $V_B$ , the  $a^\pi$  and  $e^\sigma$  levels derived from the B atoms at  $V_N$  site are

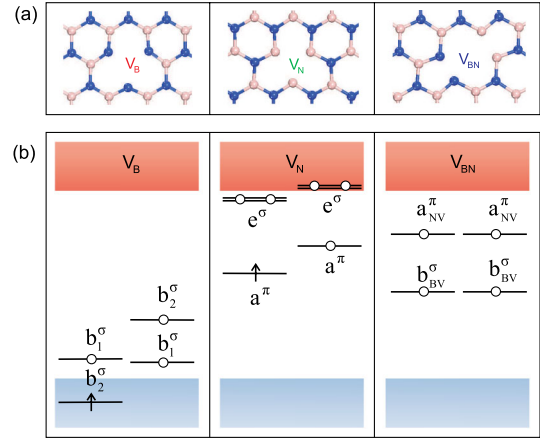


FIG. 1 (color online). (a) The (local) optimized geometries of  $V_B$ ,  $V_N$ , and  $V_{BN}$  in SLBN. (b) The schematic drawings of the in-gap defect levels induced by  $V_B$ ,  $V_N$ , and  $V_{BN}$ . The symmetry of these defect levels are explained in the text.

present in the gap and  $e^\sigma$  is close to the conduction band minimum (CBM) and the  $a^\pi$  level in spin-up channel is occupied, as shown in Fig. 1(b). The defect levels of  $V_{BN}$  could be regarded as the combination of  $V_B$  and  $V_N$ . Two unoccupied levels derived from B vacancy ( $b_{BV}^\sigma$ ) and N vacancy ( $a_{NV}^\pi$ ) at  $V_{BN}$  are present in the gap. The  $a_{NV}^\pi$  level is high in energy, making  $V_{BN}$  as a double acceptor.

Depending on the position and symmetry of in-gap levels induced by vacancies, it is expected that they can interact with the adsorbed TM  $3d$  to achieve the controllable charge and magnetic states of TM/SLBN. For instance, since the energies of TM  $3d$  orbitals are roughly located at the middle of the gap of SLBN, they could behave as  $\text{TM}^{3+}$  ion after coupling to triple-acceptor  $V_B$  or  $\text{TM}^{2+}$  ion after interact with double-acceptor  $V_{BN}$ . Since the in-gap levels induced by  $V_N$  are comparable to that of  $3d$  orbitals of TM in energy, instead of charge transfer, hybridization effect can play a critical role in determining the magnetic states of TM- $V_N$ .

When a TM atom is attached on these vacancies [Fig. 2(a)], the binding energy of a TM atom on  $V_B$  ( $-4$  to  $12$  eV) is significantly larger than that of on  $V_{BN}$  and  $V_N$ , which could be understood by the larger charge transfer effect in TM- $V_B$ . Among these TM atoms, Sc atom adsorption on  $V_B$  has the largest binding energy compared to other TM atoms on  $V_B$ , as shown in Fig. 2(b), consisting with the fact that the  $3d$  orbitals of Sc are highest in energy than other  $3d$  TM atoms and the largest energy gain could occur for Sc/SLBN during the charge transfer.

For TM atoms adsorption on  $V_{BN}$ , two electrons of TM atom transfer to  $b_{BV}^\sigma$  level of  $V_{BN}$ , giving rise to  $\text{TM}^{2+}$  charge state. The alignment of the remaining  $3d$  electrons exactly follows the Hund's rule, as shown in Fig. 2(d). For TM atoms adsorption on  $V_B$ , TM atoms exactly exhibit  $\text{TM}^{3+}$  state after three electrons transfer to the three  $b^\sigma$  levels of  $V_B$ . Similar results are found for TM adsorption

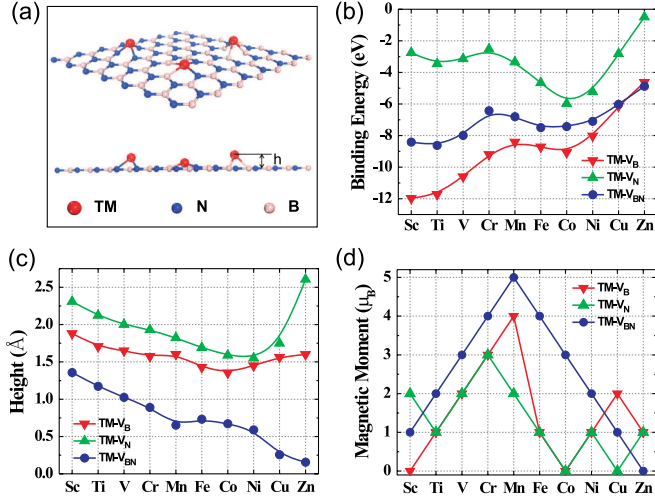


FIG. 2 (color online). (a) The schematic structure of TM atoms adsorb on  $V_B$ ,  $V_N$ , and  $V_{BN}$  in SLBN. (b) The binding energies of TM atoms adsorption on  $V_B$ ,  $V_N$ , and  $V_{BN}$  in SLBN. (c) The height of the TM atoms above the SLBN surface when TM atoms adsorb on  $V_B$ ,  $V_N$ , and  $V_{BN}$ . (d) The magnetic moments of SLBN with TM atoms adsorption on  $V_B$ ,  $V_N$ , and  $V_{BN}$ .

on cation-vacancy in other TM/III-V layers. All the TM atoms on  $V_B$  show high-spin configurations based on Hund's rule except for Fe, Co, and Ni atoms, as shown in Fig. 2(d).

In order to understand the physical mechanism of the high-spin and low-spin configurations, we have analyzed the alignment and charge transfer between TM and SLBN. Taking Cr- $V_B$  as a typical example of high-spin case, the 3d orbitals of Cr atoms are split into a single  $a^d$  ( $d_{z^2}$ ) state and two twofold degenerate  $E_1^d$  ( $d_{xy} + d_{x^2-y^2}$ ) and  $E_2^d$  ( $d_{yz} + d_{xz}$ ) states under  $C_{3V}$  symmetry.  $E_1$  and  $E_2$  are mixed and split into two peaks, defined as  $e_1^d$  and  $e_2^d$ , as shown in Figs. 3(a). After three electrons transfer to the  $V_B$   $b^\sigma$  levels, the remaining  $d^3$  orbitals of  $\text{Cr}^{3+}$  occupy the  $a^d$  and  $e_1^d$  in spin-up channel and exhibit a  $d^3t_1d^0$  high-spin configuration. The fully occupied  $V_B$   $b^\sigma$  levels are then downshifted into valence band and convert to doubly

degenerate  $e^\sigma$  state. In Cr- $V_B$ , the size of exchange splitting of  $e^d$  orbitals  $\Delta_{ex}$  is larger than that of crystal field splitting  $\Delta_{cf}$  between  $e_1^d$  and  $e_2^d$ . The same physical mechanism results in the high-spin configurations in V- $V_B$  and Mn- $V_B$ . The case is opposite for the low-spin configurations in Fe- $V_B$ , Co- $V_B$ , and Ni- $V_B$ , where  $\Delta_{cf} > \Delta_{ex}$  (Fig. 3(c)). Taking Fe- $V_B$  as an example, because  $\Delta_{cf} > \Delta_{ex}$ , the electrons transfer from  $e_2^d$  in spin-up channel to  $e_1^d$  in spin-down channel, resulting in a  $d^3t_1d^2$  low-spin configuration. The same physical mechanism results in the low-spin configurations of Co- $V_B$  and Ni- $V_B$ . Moreover, because  $e^d$  is not occupied for  $\text{Ti}^{3+}$  while  $e_1^d$  in spin-down channel is fully occupied for  $\text{Cu}^{3+}$  and  $\text{Zn}^{3+}$ , the high-spin states of Ti- $V_B$ , Cu- $V_B$ , and Zn- $V_B$  are not dependent on the relative sizes of  $\Delta_{cf}$  and  $\Delta_{ex}$ . Generally, our results can be understood by the crystal field theory based on Griffith's theory of TM ions [29].

As we learned from the Cr- $V_B$  and Fe- $V_B$  cases above, the high or low-spin configuration is mostly determined by the relative size of  $\Delta_{ex}$  and  $\Delta_{cf}$ . Thus, the transition between high-spin and low-spin configurations of TM- $V_B$  could be achieved by controlling the size of  $\Delta_{ex}$  and/or  $\Delta_{cf}$ . To confirm our physical intuition, taking Fe- $V_B$  as an example, our calculations show that if the height of Fe atom on  $V_B$  is increased from 1.42 to 1.61 Å (the total energy is increased by 0.23 eV), then  $\Delta_{cf} < \Delta_{ex}$ , and the spin of Fe transfers to the high-spin  $d^5t_1d^0$  configuration. In experiments, this spin transition might be achieved by either using a STM tip to modulate the height of TM atoms or applying a certain strain on SLBN.

The situation of TM atoms adsorption on  $V_N$  is more complicated and quite different from that of on  $V_B$  and  $V_{BN}$ . Since the position of  $V_N$  in-gap levels is comparable to that of TM 4s, 3d orbitals in energy, the covalent hybridization between  $V_N$   $a^\pi$ ,  $e^\sigma$  and TM 4s, 3d states plays the dominant role in determining the magnetic state of TM- $V_N$ . TM s,  $d_{z^2}$  orbitals belong to the a representation under  $C_{3V}$  symmetry while TM  $d_{xy, x^2-y^2, yz, xz}$  belong to the e representation. As shown in Fig. 1(b), the in-gap levels of  $V_N$  also can be classified to a and e symmetry. According

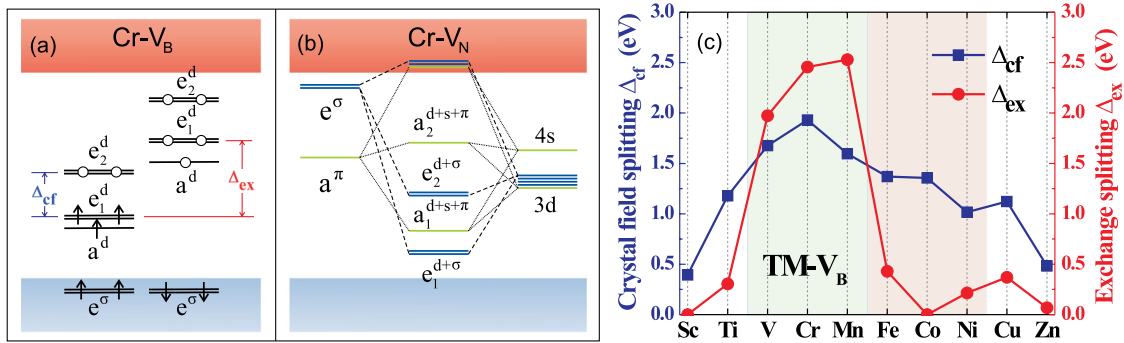


FIG. 3 (color online). (a) The schematic representation of the 3d levels of Cr atom after adsorption on  $V_B$ . The definition of the crystal field splitting  $\Delta_{cf}$  and exchange splitting  $\Delta_{ex}$  are explained in the text. (b) The schematic drawing of the symmetry-dependent coupling mechanism between  $V_N$  in-gap levels and Cr orbitals. (c) The calculated  $\Delta_{cf}$  and  $\Delta_{ex}$  of TM atoms in TM- $V_B$ .

to the orbital selection rule, TM  $s, d_{z^2}$  orbitals mostly couple with  $V_N$   $a\pi$  state due to the same representation while TM  $d_{xy, x^2-y^2, yz, xz}$  mostly couple with  $V_N$   $e^\sigma$  states. Our electronic structure calculations confirm the orbital selection rule. Taking Cr- $V_N$  as an example (Fig. 3(b)), the symmetry-dependent hybrid levels appear in the gap and are arranged in the order of  $e_1^{d+\sigma}, a_1^{d+s+\pi}, e_2^{d+\sigma}, a_2^{d+s+\pi}$  in both spin-channels. The  $e_1^{d+\sigma}, a_1^{d+s+\pi}, e_2^{d+\sigma}$  states are occupied in spin-up channel while only  $e_1^{d+\sigma}$  is occupied in spin-down channel, giving rise to a magnetic moment of  $3 \mu_B$ . From Mn to Zn, the  $a_1^{d+s+\pi}$  and  $e_2^{d+\sigma}$  hybrid states become gradually occupied in spin-down channel as well, giving rise to low-spin configurations, as shown in Fig. 2(d).

The general rule we provide here to control the charge and magnetic states of TM atoms by defect engineering is not limited to the vacancy defects but can be extended to other kinds of defects like C impurity. When C substitute N ( $C_N$ ) in SLBN [25], because C is less electronegative than N, a defect level with  $C$   $p_z$  component is pushed up above the valence band and it is occupied (unoccupied) in the spin-up (spin-down) channel [27,30]. TM atom on  $C_N$  transfers one electron to the unoccupied  $p$ -type defect level and exhibits  $TM^{1+}$  charge state. The remaining  $3d$  orbitals of TM atoms are aligned as Hund's rule. For example, Mn on  $C_N$  exhibits an orbital alignment of  $d^{5\uparrow}d^{1\downarrow}$  after one  $4s$  electron transfers to  $d^l$ .

The understanding above suggests that the magnetic properties of TM/SLBN can be tuned if we can effectively adjust the relative energy positions of TM and/or defective SLBN. For example, applying an external electric field  $E_{\text{ext}}$  can shift the relative energy level positions because TM and SLBN are not in the same plane and because TM and SLBN can have opposite charge states when SLBN is defective. Taking Mn- $V_B$  as an example (Fig. 4), Mn- $V_B$  exhibits a  $d^{4\uparrow}d^{0\downarrow}$  high-spin configuration without an  $E_{\text{ext}}$  [Fig. 2(d)]. A positive  $E_{\text{ext}}$  exerts a force on the system, pushing the Mn closer to the SLBN because Mn is positive charged and SLBN is negatively charged. This increases the crystal field splitting. Remarkably, when  $E_{\text{ext}}$  is increased to 1.0 V/nm, the height of Mn atom on  $V_B$  is decreased suddenly from  $\sim 1.6/\text{\AA}$  to  $\sim 1.5/\text{\AA}$ . The large increase of the crystal field splitting causes a spin crossover, i.e., charges are transferred from the spin-up channel to the spin-down channel [Fig. 4(c)] and the spin configuration converts from  $d^{4\uparrow}d^{0\downarrow}$  to  $d^{3\uparrow}d^{1\downarrow}$ , as shown in Fig. 4(b). This low-spin state is found to be a metastable one with a total energy of  $\sim 360$  meV higher than that of the high-spin state in the absence of  $E_{\text{ext}}$ . Therefore, a negative critical  $E_{\text{ext}}$  is required to convert the low-spin state to high-spin one to realize the controllable spin-crossover effect.

The similar physical mechanism results in the spin configuration of Co- $V_{BN}$  transfer from  $d^{3\uparrow}d^{0\downarrow}$  to  $d^{2\uparrow}d^{1\downarrow}$  when  $E_{\text{ext}}$  is about 3.0 V/nm [Fig. 4(b)]. The fact that larger  $E_{\text{ext}}$  is required for the Co- $V_{BN}$  system than the Mn- $V_B$  system is consistent with the fact that the Co- $V_{BN}$  is less

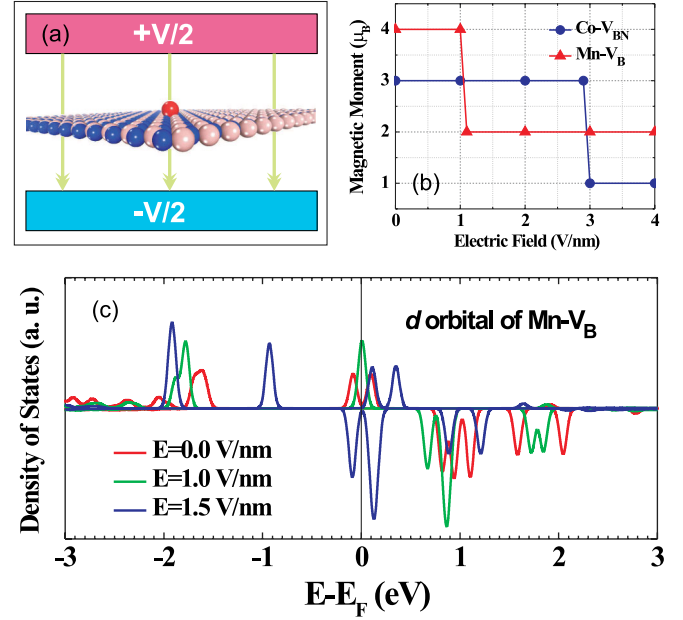


FIG. 4 (color online). (a) The model of a TM-SLBN system under an  $E_{\text{ext}}$ . An  $E_{\text{ext}}$  is oriented normally to SLBN surface and is assumed to be positive when it is directed downward. (b) The magnetic moments of Co- $V_{BN}$  and Mn- $V_B$  as a function of  $E_{\text{ext}}$ . (c) The energy shift of  $d$  orbitals for Mn- $V_B$  as a function of  $E_{\text{ext}}$ . The Fermi level is set to zero.

ionized, i.e., less charge transfer between TM and SLBN, than Mn- $V_B$ . It is worth to notice that the small critical  $E_{\text{ext}}$  in these systems indicates that it is possible to achieve this spin-crossover effect in experiments [31]. Our calculations show that this spin-crossover effect exists generally in TM/III-V and TM/II-VI layer structures, which strongly suggests that these TM/ionic-layer systems could be used for electromagnetic applications such as  $E_{\text{ext}}$ -driven nonvolatile memory devices.

In conclusion, by using DFT calculations we have demonstrated that the charge and magnetic states of TM atoms on SLBN can be effectively controlled by internal defect engineering and external electric fields. Our conclusions got from TM/SLBN systems are valid in other TM/III-V or TM/II-VI layer structures.

B. H. and S.-H. W. acknowledge the support by the U.S. Department of Energy under Contract No. DE-AC36-08GO28308. J. Y. acknowledges the support by the National Research Foundation of Korea (No. R17-2008-033-01000-0). H. X. acknowledges the support by the National Science Foundation of China, Pujiang plan, and The Program for Professor of Special Appointment (Eastern Scholar) at Shanghai Institutions of Higher Learning.

- [1] A. K. Geim and K. S. Novoselov, *Nature Mater.* **6**, 183 (2007).
- [2] M. Fujita, K. Wakabayashi, K. Nakada, and K. Kusakabe, *J. Phys. Soc. Jpn.* **65**, 1920 (1996).

- [3] C. Tao, L. Jiao, O. V. Yazyev, Y.-C. Chen, J. Feng, X. Zhang, R. B. Capaz, J. M. Tour, A. Zettl, S. G. Louie, H. Dai, and M. F. Crommie, *Nature Phys.* **7**, 616 (2011).
- [4] M. M. Ugeda, I. Brihuega, F. Guinea, and J. M. Gomez-Rodriguez, *Phys. Rev. Lett.* **104**, 096804 (2010).
- [5] N. Tombros, C. Jozsa, M. Popinciuc, H. T. Jonkman, and B. J. van Wees, *Nature (London)* **448**, 571 (2007).
- [6] R. Sielemann, Y. Kobayashi, Y. Yoshida, H. P. Gunnlaugsson, and G. Weyer, *Phys. Rev. Lett.* **101**, 137206 (2008).
- [7] V. W. Brar, R. Decker, H. Solowan, Y. Wang, L. Maserati, K. T. Chan, H. Lee, C. Girit, A. Zettl, S. G. Louie, M. L. Cohen, and M. F. Crommie, *Nature Phys.* **7**, 43 (2010).
- [8] V. M. Karpan, G. Giovannetti, P. A. Khomyakov, M. Talanana, A. A. Starikov, M. Zwierzycki, J. van den Brink, G. Brocks, and P. J. Kelly, *Phys. Rev. Lett.* **99**, 176602 (2007).
- [9] B. Uchoa, V. N. Kotov, N. M. R. Peres, and A. H. Castro Neto, *Phys. Rev. Lett.* **101**, 026805 (2008).
- [10] A. V. Krasheninnikov, P. O. Lehtinen, A. S. Foster, P. Pyykko, and R. M. Nieminen, *Phys. Rev. Lett.* **102**, 126807 (2009).
- [11] B. Huang, J. Yu, and S.-H. Wei, *Phys. Rev. B* **84**, 075415 (2011).
- [12] D. D. Awschalom and M. E. Flatte, *Nature Phys.* **3**, 153 (2007).
- [13] K. Sato, L. Bergqvist, J. Kudrnovsky, P. H. Dederichs, O. Eriksson, I. Turek, B. Sanyal, G. Bouzerar, H. Katayama-Yoshida, V. A. Dinh, T. Fukushima, H. Kizaki, and R. Zeller, *Rev. Mod. Phys.* **82**, 1633 (2010).
- [14] K. K. Kim, A. Hsu, X. Jia, S. M. Kim, Y. Shi, M. Hofmann, D. Nezich, J. F. Rodriguez-Nieva, M. Dresselhaus, T. Palacios, and J. Kong, *Nano Lett.* **12**, 161 (2012).
- [15] C. Tusche, H. L. Meyerheim, and J. Kirschner, *Phys. Rev. Lett.* **99**, 026102 (2007).
- [16] C. L. Freeman, F. Claeysens, N. L. Allan, and J. H. Harding, *Phys. Rev. Lett.* **96**, 066102 (2006).
- [17] D. Wu, M. G. Lagally, and F. Liu, *Phys. Rev. Lett.* **107**, 236101 (2011).
- [18] W. A. Harrison, *Electronic Structure and The Properties of Solids*, (Dover Publications, Mineola, NY, USA, 1989).
- [19] See Supplemental Material at <http://link.aps.org/supplemental/10.1103/PhysRevLett.108.206802> for theoretical methods and the results from hybrid functional calculations.
- [20] C. Ataca and S. Ciraci, *Phys. Rev. B* **82**, 165402 (2010).
- [21] Y. Gan, L. Sun, and F. Banhart, *Small* **4**, 587 (2008).
- [22] R. Zan, U. Bangert, Q. Ramasse, and K. S. Novoselov, *Nano Lett.* **11**, 1087 (2011).
- [23] O. Cretu, A. V. Krasheninnikov, J. A. Rodriguez-Manzo, L. Sun, R. M. Nieminen, and F. Banhart, *Phys. Rev. Lett.* **105**, 196102 (2010).
- [24] M. Gyamfi, T. Eelbo, M. Wasniowska, and R. Wiesendanger, *Phys. Rev. B* **84**, 113403 (2011).
- [25] O. L. Krivanek, M. F. Chisholm, V. Nicolosi, T. J. Pennycook, G. J. Corbin, N. Dellby, M. F. Murfitt, C. S. Own, Z. S. Szilagy, M. P. Oxley, S. T. Pantelides, and S. J. Pennycook, *Nature (London)* **464**, 571 (2010).
- [26] C. Jin, F. Lin, K. Suenaga, and S. Iijima, *Phys. Rev. Lett.* **102**, 195505 (2009).
- [27] S. Azevedo, J. R. Kaschny, C. M. C. de Castilho, and F. de Brito Mota, *Eur. Phys. J. B* **67**, 507 (2009).
- [28] C. Attaccalite, M. Bockstedte, A. Marini, A. Rubio, and L. Wirtz, *Phys. Rev. B* **83**, 144115 (2011).
- [29] J. S. Griffith, *The Theory of Transition-Metal Ions* (Cambridge University Press, Cambridge, England, 1961).
- [30] N. Berseneva, A. V. Krasheninnikov, and R. M. Nieminen, *Phys. Rev. Lett.* **107**, 035501 (2011); B. Huang and S.-H. Wei, *Phys. Rev. Lett.* **107**, 239601 (2011).
- [31] Y. Zhang, T.-T. Tang, C. Girit, Z. Hao, M. C. Martin, A. Zettl, M. F. Crommie, Y. R. Shen, F. Wang, *Nature (London)* **459**, 820 (2009).